Distributed Control of Islanded Series PV-Battery-Hybrid Systems with Low Communication Burden

Pan, Yiwei; Sangwongwanich, Ariya; Yang, Yongheng; Blaabjerg, Frede

Published in:
I E E E Transactions on Power Electronics

DOI (link to publication from Publisher):
10.1109/TPEL.2021.3063111

Publication date:
2021

Document Version
Accepted author manuscript, peer reviewed version

Citation for published version (APA):
Pan, Y., Sangwongwanich, A., Yang, Y., & Blaabjerg, F. (2021). Distributed Control of Islanded Series PV-Battery-Hybrid Systems with Low Communication Burden. *I E E E Transactions on Power Electronics*, *36*(9), 10199-10213. [9367022]. https://doi.org/10.1109/TPEL.2021.3063111

Distributed Control of Islanded Series PV-Battery-Hybrid Systems with Low Communication Burden

Yiwei Pan, *Graduate Student Member, IEEE*, Ariya Sangwongwanich, *Member*, *IEEE*, Yongheng Yang, *Senior Member, IEEE*, and Frede Blaabjerg, *Fellow, IEEE*

***Abstract*- The series photovoltaic-battery-hybrid (PVBH) system is considered as a promising solution to better integrating distributed energy sources. However, the state-of-the-art controls are either highly dependent on the communication, by which real-time control variables should be transmitted among all converters, or only suitable for PVBH systems with unity power factor. Accordingly, a novel distributed control is proposed for islanded PVBH systems in this paper. Firstly, a *PQ* decoupling control is introduced, enabling the control of individual converters with only local measurements. Then, a droop controller is implemented in the battery converter, allowing the system to participate in regulating the islanded grid (voltage and frequency). A reactive power distribution method is subsequently introduced to equalize power sharing among the converters. Additionally, two anti-over-modulation loops are developed to address the over-modulation issue of both PV converters and the battery converter. With the proposed method, only a few variables with very slow dynamics should be transmitted, and the communication burden can be significantly reduced, leading to higher reliability to some extent. Experimental results have validated the effectiveness of the proposal.**

***Index Terms*- Distributed control, power control, series-connected converters, PV-battery systems, communication.**

I. Introduction

In recent years, series configurations have gained more interest in integrating distributed energy sources [1]-[7]. With this, distributed low-voltage (LV) resources can be directly interfaced to separate DC rails of the series converter without an additional boost stage [2]. This will bring several benefits to the entire distributed system, e.g., reduced cost, improved efficiency, and modular design. However, in most applications, the series system was controlled in a centralized way which requires high-bandwidth communication [3]-[6] to exchange physical information and gating signals between the central controller and distributed converters. This significantly increases the cost and reduces the reliability of the distributed system. Therefore, efforts have been made towards the distributed/decentralized control of series distributed systems [2], [7]-[18].

Manuscript received November 10, 2020; revised January 23, 2021; accepted February 25, 2021. This work was supported by the research project – Reliable Power Electronic based Power Systems (REPEPS) by THE VELUX FOUNDATIONS under Award Ref. No.: 00016591. *(Corresponding Author: Yongheng Yang.)*

Y. Pan, A. Sangwongwanich, and F. Blaabjerg are with the Department of Energy Technology, Aalborg University, Aalborg 9220, Denmark (e-mail: ypa@et.aau.dk; ars@et.aau.dk; fbl@et.aau.dk).

Y. Yang is with the College of Electrical Engineering, Zhejiang University, Hangzhou 310027, China (e-mail: yang_yh@zju.edu.cn)

State-of-the-art distributed/decentralized control methods can be categorized as: 1) communication-based and 2) communication-free. A typical communication-based control was proposed in [2] to achieve power scheduling for series systems. In this control, a central controller is responsible for the voltage control of the point of common coupling (PCC), and local controllers are in charge of the power regulation of individual converters. However, it is highly dependent on the low-bandwidth communication (LBC) system, by which many control variables should be transmitted in real-time between the central and local controllers, leading to poor fault tolerant capability and reliability. In [8], a distributed power control method was proposed for grid-connected series PV systems, where each converter can be individually controlled without the central controller. However, the control of each converter relies on the information of the grid phase-angle, which should either be transmitted in real-time by the LBC, or sampled by additional voltage sensors for all converters, making this solution not cost-effective, especially when many converters are used. Then, the current-/voltage-mode (CVM) control scheme was developed [9]-[12], where one or several converters are centrally controlled as a current source to regulate the line current of the series system, and others in a distributed way as voltage sources. With this, the communication burden can be reduced to some extent [12]. Nevertheless, only the grid-connected operation with unity power factor (PF) was addressed in this method, while the islanded operation has not been studied. In this case, certain converters may easily suffer from overloading or even over-modulation if the load reactive power is not properly distributed. It may eventually lead to severer voltage distortion or even system instability.

To avoid the LBC, several communication-free methods have been proposed for series systems [13]-[17]. For instance, an inverse PF droop control and frequency-active/reactive power (*f*-*P*/*Q*) droop control were proposed in [13] and [14], respectively. Nevertheless, in these methods, only ideal or identical DC sources with equal power sharing are considered, When different types of DC sources (e.g., PV panels and batteries) are interfaced to each DC rail, or the active/reactive power sharing is unequal, these methods cannot be directly implemented. It means that the application of these communication-free control methods is limited in practice. Subsequently, other communication-free methods have been developed with the introduction of the LBC. For example, in [18], an LBC-dependent two-layer coordinated power control based on the inverse PF droop control was introduced to

TABLE I
STATE-OF-THE-ART DISTRIBUTED/DECENTRALIZED CONTROL METHODS FOR SERIES SYSTEMS.

Reference	Types of DC sources	Control architecture		Communication burden	Operating condition	Application limitations when applying to series PVBH systems		Over-modulations
[20], [21]	PV panels and batteries	Two-layer hierarchical control		High	Grid-connected operation with variable PF	Highly dependent on the LBC; control-related variables should be real-time transmitted		Over-modulation issue addressed only for PV converters
[8]	PV panels	Distributed *PQ* control		Low	Grid-connected operation with variable PF	Additional PCC voltage sensor for each converter; same-type DC sources; reactive power distribution is not addressed		Not addressed
[12]	Ideal DC sources	CVM control		Low	Grid-connected operation with unity PF	Additional PCC voltage sensor for each converter	Reactive power distribution is not considered	Not addressed
[9]	PV panels			Low		Same-type DC sources		
[11]	PV panels and batteries			Low				
[22]	PV panels and batteries		*P*-*V* and PF-*ω* control for PV converters	Communication -free				
[13]	Ideal DC sources	Inverse droop control		Communication -free	Islanded operation with RL loads	Only suitable for RL loads	Amplitude of the output AC voltage reference for each converter is fixed; only ideal DC sources with equal power sharing are considered	Not addressed
[14]		*f*-*P*/*Q* droop control			Islanded operation at quadrant I and IV	Mathematically unfeasible for pure resistance loads		
[15]		*P*-*ω* droop control			Grid-connected operation			
[16]		PF angle droop control			Grid-connected and islanded operation			
[17]	DC capacitors	*Q*-*ω* and *P*-*V* control			Grid-connected operation with PF close to 0	Specially designed for STATCOM; Only effective when the PFs of all converters are close to 0		Not addressed
[18]	batteries	two-layer cascaded droop and inverse droop control		Low	Grid-connected and islanded operation	Rely on the central controller and LBC to generate and transmit frequency, voltage amplitude and power references; specially designed for battery systems		Not addressed
[23]	PV panels and a dispatchable source (can be batteries)	Autonomous *PQ* control for individual converters		Communication -free	Islanded operation at quadrant I and IV	Poor PV power utilization when the PF of the entire series system is small; overloading possibility of the dispatchable converter		Not addressed

series-connected energy-storage systems, where unequal active/reactive power sharing has been achieved according to the state-of-charge (SoC) of each battery. This indicates that although the LBC can be avoided in certain applications, the LBC is usually indispensable due to various factors and practical working conditions. Moreover, as it has been recommended in IEEE Standard 1547-2018, distributed energy resources shall be capable of communicating to support the information exchange [19]. Therefore, the LBC is necessary for series systems. In all, these communication-free methods can be good candidates to reduce the communication burden.

On the other hand, since energy storage elements such as batteries can be equipped with PV systems to compensate for the fluctuation of solar energy, the series PV-battery-hybrid (PVBH) systems have been discussed recently [3], [11], [20]-[22]. Based on the hierarchical control structure in [1], power control and management methods were developed to achieve schedulable power for the series PVBH systems in [20] and [21], while ensuring a good harvesting of the PV power. The grid-connected operation of the PVBH system has also been discussed in [11] and [22] using the CVM control, where a ramp-rate and a virtual inertia control have been proposed for the battery cell to mitigate PV power variations, respectively. However, as the methods are similar to those in [9] and [12], the challenging issues remain in the control. In [23], an autonomous power control scheme has been developed for islanded series systems, where PV panels and dispatchable sources are interfaced. Yet, the PFs of PV converters are always kept consistent with the entire system, which may lead to poor PV power utilization, and potential overloading of the dispatchable converter. That is, the power distribution and utilization are not optimized.

To summarize, there are certain limitations when implementing the above reviewed methods in series PVBH systems, as listed in Table I and detailed as follows:

1) According to previous studies, the hierarchical control and the CVM control have been applied to series

PVBH systems. However, the hierarchical control is highly dependent on the LBC, as discussed in [20] and [21], while the CVM control only deals with the grid-connected operation with unity PF [11], [22].

2) Although the two-layer control in [18] based on the inverse PF droop control can cope with unequal active and reactive power sharing, it still relies on the central controller to generate the frequency reference for all converters, indicating that the system is highly LBC-dependent. Moreover, this approach is designed for the series system with the same type of DC sources, i.e., not suitable for series PVBH systems. In addition, certain communication-free control schemes are designed for special applications. For instance, the reactive power versus angular frequency (Q-ω) and active power versus AC voltage amplitude (P-V) control proposed in [17], where the PFs of all converters are close to 0, are not applicable to PVBH systems.

3) Over-modulation of individual converters is one common issue in the series system, which may be induced by the unbalanced power sharing among the series converters, and possibly lead to instability and performance degradation of the system [24]. However, in the control methods discussed above, it has rarely been addressed except in [21], where only the over-modulation of PV converters is considered. In fact, all converters may suffer from over-modulation, and the anti-over-modulation (AOM) strategies for all converter cells should be further studied to ensure the stable operation of the series PVBH system.

4) Islanded operation of the series PVBH system has rarely been discussed. On one hand, the control objectives of the grid-connected operation with unity PF are maximizing the power utilization from PV converters, while using the battery converter to improve the power quality and enhance the stability of the system [11], [12], [20], [21]. On the other hand, for the islanded operation, the priority of the system is to fulfil the load demands with the participation of all converters, while maintaining the islanded grid voltage and frequency. With this goal, the system should extract as much power from the PV converters as possible, and properly distribute the reactive power among all converters. Therefore, the islanded operation requires further exploration.

To overcome those limitations, the islanded operation of the series PVBH system with a novel distributed control is discussed in this paper. With the proposed control, the PV panels can harvest as much power as possible, while the battery automatically regulates the voltage and frequency of the islanding grid according to the load demand. Moreover, reactive power can be shared to balance the loading of all converters. To guarantee the stable operation of the system, two AOM loops are developed. In the proposed control, only the total active and reactive power, active power of each converter, and the amplitude of the modulation index for the battery converter with low dynamics should be transmitted through the LBC system, significantly reducing the communication burden.

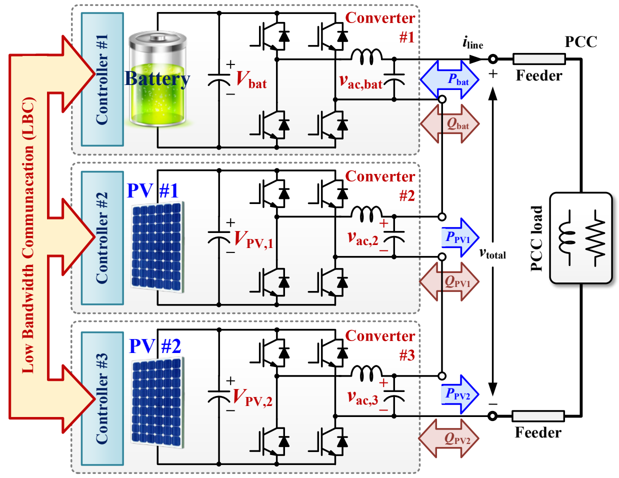

Fig. 1. Hardware schematic of a 3-cell series PVBH system, where $v_{ac,k}$ and $v_{ac,bat}$ are the AC voltages of the k^{th} converter cell and the battery cell, respectively, $V_{PV,m}$ and V_{bat} are the DC voltages of PV #m and the battery, respectively, and v_{total} is the output voltage of the system.

The rest of this paper is organized as follows. In Section II, a PQ decoupling control is proposed, enabling the individual active and reactive power control with only local measurements. Then, the droop control is implemented for the battery converter. A reactive power distribution method is developed to realize approximately equal power sharing of all converters. In Section III, a small-signal analysis is conducted. In Section IV, the over-modulation issues of the series PVBH system is analyzed, and the AOM loops are developed. The effectiveness of the proposed distributed control is then validated by experimental tests in Section V. Finally, concluding remarks are provided in Section VI.

II. Proposed Distributed Control

A. *PQ Decoupling Control for PV Converters*

To illustrate the proposed control, an islanded 3-cell series PVBH system is shown in Fig. 1, where two PV converters and one battery converter are connected in series. In the following analysis, only one battery converter is considered for simplicity. It can be observed that the same line current i_{line} flows through all cells, while the output voltage of each cell can be different both in amplitude and phase angle. The corresponding phasor diagram is shown in Fig. 2, where the grid voltage vector $\dot{V}_{total}$ is synthesized by voltage vectors $\dot{V}_1$, $\dot{V}_2$ and $\dot{V}_3$. As shown in Fig. 2, the increment of $|\dot{V}_1|$ (the amplitude of $\dot{V}_1$) will lead to the increase of both active and reactive power of the k^{th} cell (k refers to one of the specific cells), while the increase of the PF angle θ_1 will result in the decrease of the active power and increase of the reactive power. According to Fig. 2, assuming that the increments on the AC voltage amplitude and PF angle of the k^{th} converter (denoted by ΔV_k and $\Delta\theta_k$, respectively) are very small, the output power variation for the k^{th} cell can be obtained as

$$\begin{bmatrix}\Delta P_k\\ \Delta Q_k\end{bmatrix} = I_{line}\begin{bmatrix}\cos\theta_k & -V_k\sin\theta_k\\ \sin\theta_k & V_k\cos\theta_k\end{bmatrix}\begin{bmatrix}\Delta V_k\\ \Delta\theta_k\end{bmatrix} = I_{line}A\begin{bmatrix}\Delta V_k\\ \Delta\theta_k\end{bmatrix} \quad (1)$$

where θ_k and V_k are the PF angle and AC voltage amplitude of the k^{th} converter, respectively, ΔP_k and ΔQ_k are the increments of the active power and reactive power of the k^{th} converter, respectively, and A is the coupling matrix. From (1), it can be observed that the variation of ΔV_k and $\Delta\theta_k$ will affect both the active and reactive power. This coupling relationship is dependent on the power factor of the k^{th} cell. Therefore, different from the parallel distributed power converters, the well-known active power versus frequency (P-f) and reactive power versus voltage (Q-V) droop control cannot be directly implemented to individually control the converters. It thus calls for distributed control methods.

By solving the inverse matrix of A, it gives

$$\begin{bmatrix}\Delta V_k\\ \Delta\theta_k\end{bmatrix} = \frac{A^{-1}}{I_{line}}\begin{bmatrix}\Delta P_k\\ \Delta Q_k\end{bmatrix} = \frac{1}{I_{line}}\begin{bmatrix}\cos\theta_k & \sin\theta_k\\ -\dfrac{\sin\theta_k}{V_k} & \dfrac{\cos\theta_k}{V_k}\end{bmatrix}\begin{bmatrix}\Delta P_k\\ \Delta Q_k\end{bmatrix}. \quad (2)$$

To regulate the individual active/reactive power of each cell, a *PQ* decoupling control can be obtained according to (2), as shown in Fig. 3(a), being the overall control diagram of the PV converter. As shown in Fig. 3(a), the active power of the PV converter is regulated by controlling the PV voltage V_{PV} or power P_{PV}, with a maximum power point tracking (MPPT) controller. Both the active power (or DC voltage) and reactive power are regulated by proportional-integral (PI) controllers, and through the decoupling matrix, the increments on the amplitude and frequency of the output voltage can be calculated. The output voltage reference of the k^{th} converter, which is denoted as $v^*_{ac,k}$, is calculated by

$$v^*_{ac,k} = V^*_k\sin\left(\int\omega^*_k dt\right) = \left(\frac{V_{g,nom}}{n} + \Delta V_k\right)\sin\left(\int(\omega_{nom} + \Delta\omega_k)\,dt\right) \quad (3)$$

where $V_{g,nom}$ and ω_{nom} are the nominal amplitude and frequency of the grid voltage, respectively, n is the total number of converter cells in the series system, and $\Delta\omega_k$ is the increment on the angular frequency of the output voltage. Through the conventional voltage and current dual-loop control, both MPPT and reactive power control can be realized with only local measurements, as shown in Fig. 3(a).

B. Droop Control for the Battery Converter

As the system should participate in grid regulation while compensating for the PV power variations, the control diagram of the battery cell can thus be designed, as shown in Fig. 3(b), where the droop control is adopted. The amplitude and frequency references of the entire system, denoted as ω^*_{total} and V^*_{total}, respectively, are obtained as

$$\begin{cases}\omega^*_{total} = \omega_{total,0} - k_{D,p}P_{total}\\ V^*_{total} = V_{total,0} - k_{D,q}Q_{total}\end{cases} \quad (4)$$

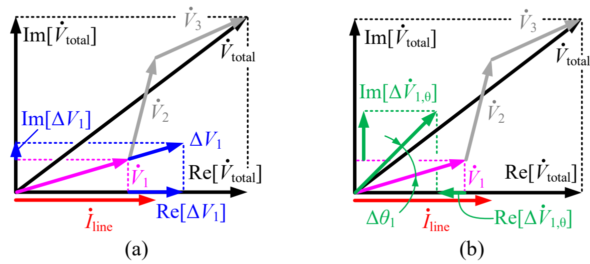

Fig. 2. Phasor diagram of a 3-cell series system shown in Fig. 1 when (a) the output voltage amplitude of converter #1 varies, and (b) the phase angle of converter #1 varies.

in which $\omega_{total,0}$ and $V_{total,0}$ are the output voltage angular frequency and amplitude at no load, and $k_{D,p}$ and $k_{D,q}$ are the droop coefficients for the frequency and amplitude, respectively. Then, the voltage reference for the entire system is calculated by

$$v^*_{total} = V^*_{total}\sin\left(\int\omega^*_{total}dt\right). \quad (5)$$

Through the voltage and current dual-loop control, the output voltage of the system can be maintained by the battery converter. In this way, the external characteristics of the series system will behave like a droop-controlled power source, while the battery operates as a buffer to compensate for the power difference between the load and the PV generation.

C. Reactive Power Distribution

The reactive power of the system is distributed to equalize the apparent power sharing among all converters. To reduce the communication burden, in the proposed approach, only the total active and reactive power are transmitted by the LBC. Then, each converter only knows its own power and the total power of the system. In this case, the reactive power reference of each converter can be decided by assuming: 1) the apparent power for all converter cells is identical, and 2) the voltage phasors of other converter cells synthesize the total voltage phasor with the minimum amplitudes. Accordingly, the relationship between the power of the PV converter and the total power can be described as

$$\frac{\left|P_k + jQ_k\right|}{\left|(P_{total} - P_k) + j(Q_{total} - Q_k)\right|} = \frac{1}{n-1} \quad (6)$$

which is also presented in Fig. 4. By solving (6), the reactive power reference can be obtained as

$$Q^*_k = \begin{cases}0, & \sigma \le 0\\ \dfrac{\sqrt{\sigma} - Q_{total}}{n^2 - 2n}, & \sigma > 0 \text{ and } \left|\sqrt{\sigma} - Q_{total}\right| < \left|-\sqrt{\sigma} - Q_{total}\right|\\ \dfrac{-\sqrt{\sigma} - Q_{total}}{n^2 - 2n}, & \sigma > 0 \text{ and } \left|\sqrt{\sigma} - Q_{total}\right| > \left|-\sqrt{\sigma} - Q_{total}\right|\end{cases}, \quad (7)$$

with

$$\sigma = Q^2_{total} - (n^2 - 2n)\left[(n-1)^2P^2_k - (P_{total} - P_k)^2 - Q^2_k\right]. \quad (8)$$

Moreover, the reactive power reference should be limited in a certain range as

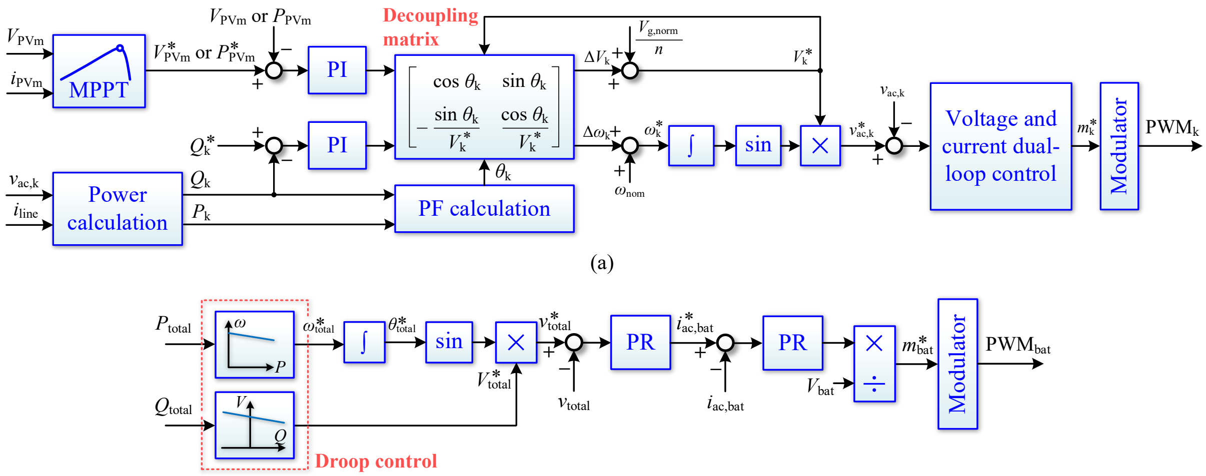

Fig. 3. Control diagrams of (a) the PV converter and (b) the battery converter. Here, the subscript "PVm" denotes the PV #m in Fig. 1, θ^*_{total} is the integration of ω^*_{total}, and PWM_k and PWM_{bat} are the pulse-width-modulation (PWM) signals for the k^{th} converter and the battery converter, respectively, m^*_k and m^*_{bat} are the modulation indices for the k^{th} converter and the battery converter, respectively, and PR represents the proportional-resonant control.

$$Q^*_\text{k} = \begin{cases} Q_{\text{total}}, \text{ if abs}(Q_{\text{total}}) < \text{abs}(Q^*_\text{k}) \\ 0, \text{ if sgn}(Q_{\text{total}}) \neq \text{sgn}(Q^*_\text{k}) \end{cases} \tag{9}$$

where abs(·) refers to the absolute value, and sgn(·) refers to the sign value. The reactive power limit in (9) is to avoid excessive and reversed reactive power contribution.

In fact, the voltage phasors of other converters cannot exactly be the phasors with minimum amplitudes, as shown in Fig. 4. Consequently, with the reactive power control in (7)−(9), the power loading of the battery cell may be higher than that for the PV converters. To address this, the integer n in (7)−(9) can be replaced by a reactive power distribution coefficient h ($h \leq n$), which can be set as either an integer or a non-integer. For instance, if h = 2.8 for a 3-cell system, through (7)−(9), the calculated Q^*_k will become higher than the case when $h = n$. In this way, the PV converters can contribute more reactive power, and the loading for the battery cell can be reduced. Moreover, h can be online adjusted to realize optimal reactive power distribution, while considering many other factors, e.g., ambient temperature and surplus power capacity of each converter. Regarding the design of h, in practice, h can be set as a constant of n, which will still be sufficient for most cases.

With the above-discussed distributed control, individual active/reactive power control, islanded and grid-tied operation, and power management considering battery SoC and reactive power distribution can be achieved for the series PVBH system. Compared with the conventional methods in [2], [20], [21], the proposed control can be realized with very low communication burden, where only the total active/reactive power and the power limiting command should be transmitted by the LBC. Since these variables are not for real-time control, the fault tolerance of the LBC can be improved.

D. Fault tolerant operation under communication failure

In practice, the system may encounter communication faults like communication jamming, data error or loss, etc. Since the

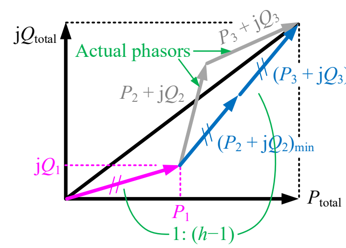

Fig. 4. Illustration of the reactive power distribution, where the subscript "min" indicates the phasor being with the minimum amplitude.

transmitted data in the proposed method are not for real-time control, more data can be transmitted within the limited communication bandwidth to enhance the reliability of the communication. For instance, certain advanced methods can be adopted, such as adding multiple error check codes, adding redundant or duplicated data, etc. to enhance the communication reliability. However, it can still be possible when some communication nodes fail due to hardware or software issues. Thus, it is necessary to discuss the fault tolerant operation of the series system under communication failure.

If the communication of certain PV converters fails, these PV converters will only be able to receive local information, while other converters can also know about the status of failed converters using approaches like heart-beat and hand-shaking signals. Consequently, only active power will be provided by these communication-failed PV converters, and their reactive power reference will be set as 0. The reactive power droop coefficient in the battery converter will be increased to reduce the reactive power capacity of the entire system, thus avoiding potential overloading of other converters. More specifically, the reactive power droop coefficient $k_{\text{D,q}}$ will be increased from $\Delta V_{\text{total}}/(2Q_{\text{max}})$ to $n \cdot \Delta V_{\text{total}}/[2(n-n_\text{f})Q_{\text{max}}]$, as shown in Fig. 5, where n_f is the number of communication-failed PV converters. In this way, the reactive power capacity of the system will be reduced to $(n-n_\text{f})/n$ times of the normal

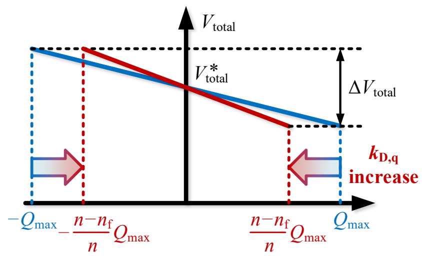

Fig. 5. Modification of the reactive power droop coefficient when the number of communication-failed PV converters is n_{f}.

system. If the communication of the battery converter fails, no PV converters will receive any information through the LBC. Then, n_{f} will be set as $(n-1)$, indicating that only the battery converter will provide the reactive power support.

III. Small-Signal Analysis

To investigate the stability of the proposed control, a small signal analysis is conducted for an n-cell PVBH system with $(n-1)$ PV converters and one battery converter. In general, the power loops and the inner voltage/current loops can be considered well-decoupled, since the power loops always have lower dynamics than the inner loops [13]. Therefore, to discuss the stability of the power loops, voltage/current tracking errors are neglected.

Based on the PQ decoupling control diagram in Fig. 3(a), the variations of the voltage amplitude and phase-angle of the k^{th} converter can be obtained as

$$\begin{bmatrix}\Delta V_{\text{k}}\\ \Delta\theta_{\text{k}}\end{bmatrix}=\begin{bmatrix}F_{11,\text{k}} & F_{12,\text{k}}\\ F_{21,\text{k}} & F_{22,\text{k}}\end{bmatrix}\begin{bmatrix}\Delta P_{\text{k}}\\ \Delta Q_{\text{k}}\end{bmatrix} \tag{10}$$

where $F_{11,\text{k}}=-\left(k_{\text{p,p}}+\frac{k_{\text{i,p}}}{s}\right)\cos\theta_{\text{k}}$, $F_{12,\text{k}}=-\left(k_{\text{p,q}}+\frac{k_{\text{i,q}}}{s}\right)\sin\theta_{\text{k}}$,

$F_{21,\text{k}}=\left(k_{\text{p,p}}+\frac{k_{\text{i,p}}}{s}\right)\sin\theta_{\text{k}}\Big/sV_{\text{k}}$, and $F_{22,\text{k}}=-\left(k_{\text{p,q}}+\frac{k_{\text{i,q}}}{s}\right)\cos\theta_{\text{k}}\Big/sV_{\text{k}}$.

Here, $k_{\text{p,p}}$, $k_{\text{i,p}}$, $k_{\text{p,q}}$, and $k_{\text{i,q}}$ are the proportional and integral gains for the active power and reactive power control loops, respectively. For the islanded operation, the active and reactive power of the k^{th} converter can be calculated as

$$\begin{aligned}P_{\text{k}}+jQ_{\text{k}}&=V_{\text{k}}e^{j\theta_{\text{k}}}\left[\left(V_{\text{total}}e^{j\theta_{\text{total}}}-V_{\text{g}}e^{j0}\right)\Big/|Z_{\text{f}}|e^{j\theta_{\text{f}}}\right]^*\\&=\frac{V_{\text{k}}}{|Z_{\text{f}}|}\left[V_{\text{total}}\cos\left(\theta_{\text{k}}-\theta_{\text{total}}+\theta_{\text{f}}\right)-V_{\text{g}}\cos\left(\theta_{\text{k}}+\theta_{\text{f}}\right)\right]\\&\quad+j\frac{V_{\text{k}}}{|Z_{\text{f}}|}\left[V_{\text{total}}\sin\left(\theta_{\text{k}}-\theta_{\text{total}}+\theta_{\text{f}}\right)-V_{\text{g}}\sin\left(\theta_{\text{k}}+\theta_{\text{f}}\right)\right]\end{aligned} \tag{11}$$

where $|Z_{\text{f}}|$ and θ_{f} refer to the amplitude and phase-angle of the feeder impedance, respectively. According to (11), the variations of the measured active and reactive power of the k^{th} converter can be derived as

$$\begin{bmatrix}\Delta P_{\text{k}}\\ \Delta Q_{\text{k}}\end{bmatrix}=G_{\text{LPFk}}(s)\begin{bmatrix}\alpha_{\text{P1,k}} & \alpha_{\text{P2,k}} & \alpha_{\text{P3,k}} & \alpha_{\text{P4,k}}\\ \alpha_{\text{Q1,k}} & \alpha_{\text{Q2,k}} & \alpha_{\text{Q3,k}} & \alpha_{\text{Q4,k}}\end{bmatrix}\begin{bmatrix}\Delta E_{\text{k}}\\ \Delta\theta_{\text{k}}\\ \Delta V_{\text{total}}\\ \Delta\theta_{\text{total}}\end{bmatrix} \tag{12}$$

in which the coefficients are expressed as

$$\begin{bmatrix}\alpha_{\text{P1,k}}\\ \alpha_{\text{P2,k}}\\ \alpha_{\text{P3,k}}\\ \alpha_{\text{P4,k}}\\ \alpha_{\text{Q1,k}}\\ \alpha_{\text{Q2,k}}\\ \alpha_{\text{Q3,k}}\\ \alpha_{\text{Q4,k}}\end{bmatrix}=\frac{1}{|Z_{\text{f}}|}\begin{bmatrix}V_{\text{total}}\cos\left(\theta_{\text{k}}-\theta_{\text{total}}+\theta_{\text{f}}\right)-V_{\text{g}}\cos\left(\theta_{\text{k}}+\theta_{\text{f}}\right)\\ V_{\text{k}}\left[-V_{\text{total}}\sin\left(\theta_{\text{k}}-\theta_{\text{total}}+\theta_{\text{f}}\right)+V_{\text{g}}\sin\left(\theta_{\text{k}}+\theta_{\text{f}}\right)\right]\\ V_{\text{k}}\cos\left(\theta_{\text{k}}-\theta_{\text{total}}+\theta_{\text{f}}\right)\\ V_{\text{k}}V_{\text{total}}\sin\left(\theta_{\text{k}}-\theta_{\text{total}}+\theta_{\text{f}}\right)\\ V_{\text{total}}\sin\left(\theta_{\text{k}}-\theta_{\text{total}}+\theta_{\text{f}}\right)-V_{\text{g}}\sin\left(\theta_{\text{k}}+\theta_{\text{f}}\right)\\ V_{\text{k}}\left[V_{\text{total}}\cos\left(\theta_{\text{k}}-\theta_{\text{total}}+\theta_{\text{f}}\right)-V_{\text{g}}\cos\left(\theta_{\text{k}}+\theta_{\text{f}}\right)\right]\\ V_{\text{k}}\sin\left(\theta_{\text{k}}-\theta_{\text{total}}+\theta_{\text{f}}\right)\\ -V_{\text{k}}V_{\text{total}}\cos\left(\theta_{\text{k}}-\theta_{\text{total}}+\theta_{\text{f}}\right)\end{bmatrix}. \tag{13}$$

Moreover, $G_{\text{LPFk}}(s)$ is an equivalent low pass filter (LPF) induced by the power measurement for the k^{th} converter, which can be approximated as $G_{\text{LPFk}}(s)=\omega_{\text{cut,k}}\big/\left(s+\omega_{\text{cut,k}}\right)$ with $\omega_{\text{cut,k}}$ being its cut-off frequency.

Considering the battery converter, the characteristic of the PVBH system behaves as a droop-controlled voltage source. The variations of the voltage amplitude and phase-angle of the battery converter can be obtained as

$$\begin{cases}\Delta V_{\text{total}}=-\Delta Q_{\text{total}}k_{\text{D,q}}\\ \Delta\theta_{\text{total}}=\dfrac{\Delta\omega_{\text{total}}}{s}=-\Delta P_{\text{total}}k_{\text{D,p}}\dfrac{1}{s}\end{cases}. \tag{14}$$

Then, the total power of the system can be calculated as

$$\begin{aligned}P_{\text{total}}+jQ_{\text{total}}&=V_{\text{total}}e^{j\theta_{\text{total}}}\left[\left(V_{\text{total}}e^{j\theta_{\text{total}}}-V_{\text{g}}e^{j0}\right)\Big/\left(|Z_{\text{f}}|e^{j\theta_{\text{f}}}\right)\right]^*\\&=\left[V_{\text{total}}^2\cos\theta_{\text{f}}-V_{\text{total}}V_{\text{g}}\cos\left(\theta_{\text{total}}+\theta_{\text{f}}\right)\right]\Big/|Z_{\text{f}}|\\&\quad+j\left[V_{\text{total}}^2\sin\theta_{\text{f}}-V_{\text{total}}V_{\text{g}}\sin\left(\theta_{\text{total}}+\theta_{\text{f}}\right)\right]\Big/|Z_{\text{f}}|\end{aligned}. \tag{15}$$

Accordingly, the variations of the measured total active and reactive power can be expressed as

$$\begin{bmatrix}\Delta P_{\text{total}}\\ \Delta Q_{\text{total}}\end{bmatrix}=\frac{G_{\text{LPF,total}}(s)}{|Z_{\text{f}}|}\cdot\begin{bmatrix}2V_{\text{total}}\cos\theta_{\text{f}}-V_{\text{g}}\cos\left(\theta_{\text{total}}+\theta_{\text{f}}\right) & V_{\text{total}}V_{\text{g}}\sin\left(\theta_{\text{total}}+\theta_{\text{f}}\right)\\ 2V_{\text{total}}\sin\theta_{\text{f}}-V_{\text{g}}\sin\left(\theta_{\text{total}}+\theta_{\text{f}}\right) & -V_{\text{total}}V_{\text{g}}\cos\left(\theta_{\text{total}}+\theta_{\text{f}}\right)\end{bmatrix}\begin{bmatrix}\Delta V_{\text{total}}\\ \Delta\theta_{\text{total}}\end{bmatrix} \tag{16}$$

where $G_{\text{LPF,total}}(s)$ is the LPF in the power measurement to avoid power oscillations in the droop control, described as $G_{\text{LPF,total}}(s)=\omega_{\text{cut,total}}\big/\left(s+\omega_{\text{cut,total}}\right)$ with $\omega_{\text{cut,total}}$ being the cut-off frequency.

Then, the power control dynamic of the system can be described by a closed-loop matrix as

$$\begin{bmatrix}A_{1,1} & A_{1,2} & \cdots & 0 & 0 & A_{1,2n-1} & A_{1,2n}\\ A_{2,1} & A_{2,2} & \cdots & 0 & 0 & A_{2,2n-1} & A_{2,2n}\\ \vdots & \vdots & \ddots & \vdots & \vdots & \vdots & \vdots\\ 0 & 0 & \cdots & A_{2n-3,2n-3} & A_{2n-3,2n-2} & A_{2n-3,2n-1} & A_{2n-3,2n}\\ 0 & 0 & \cdots & A_{2n-2,2n-3} & A_{2n-2,2n-2} & A_{2n-2,2n-1} & A_{2n-2,2n}\\ 0 & 0 & \cdots & 0 & 0 & A_{2n-1,2n-1} & A_{2n-1,2n}\\ 0 & 0 & \cdots & 0 & 0 & A_{2n,2n-1} & A_{2n,2n}\end{bmatrix}\begin{bmatrix}\Delta V_1\\ \Delta\theta_1\\ \vdots\\ \Delta V_{n-1}\\ \Delta\theta_{n-1}\\ \Delta V_{\text{total}}\\ \Delta\theta_{\text{total}}\end{bmatrix}=0 \tag{17}$$

where the elements in the coefficient matrix are expressed as

TABLE II
PARAMETERS OF THE SERIES PVBH SYSTEM.

Circuit parameter	Value
Total feeder impedance	$(0.02 + j0.1)\ \Omega$
Amplitude of the nominal grid voltage $V_{g,nom}$	311 V
Nominal grid frequency ω_{nom}	$2\pi\cdot 50$ rad/s
Initial output voltage amplitudes for PV converters	$V_1 = V_2 = 103.7$ V
Initial phase angle for the series system	$\theta_{total} = 0.02$ rad/s
Initial phase angles for PV converters	$\theta_1 = \theta_2 = 0.02$ rad/s
Control parameters	**Value**
Power control parameters for PV converters	$k_{p,p} = k_{p,q} = 0.12$ $k_{i,p} = k_{i,q} = 0.4$
Cut-off angular frequency of $G_{LPFk}(s)$	$\omega_{cut,k} = 100$ rad/s
Cut-off angular frequency of $G_{LPF,total}(s)$	$\omega_{cut,total} = 50$ rad/s
P/f Droop coefficient $k_{D,p}$	$2\pi\cdot 10^{-5}$ rad/W
Q/V Droop coefficient $k_{D,q}$	0.005 V/var

$$\begin{bmatrix} A_{2k-1,2k-1} \\ A_{2k,2k-1} \\ A_{2k-1,2k} \\ A_{2k,2k} \\ A_{2k-1,n-1} \\ A_{2k,n-1} \\ A_{2k-1,2n} \\ A_{2k,2n} \end{bmatrix} = \begin{bmatrix} F_{11,k}\alpha_{P1,k} + F_{12,k}\alpha_{Q1,k} - 1 \\ F_{21,k}\alpha_{P1,k} + F_{22,k}\alpha_{Q1,k} \\ F_{21,k}\alpha_{P2,k} + F_{12,k}\alpha_{Q2,k} \\ F_{21,k}\alpha_{P2,k} + F_{22,k}\alpha_{Q2,k} - 1 \\ F_{11,k}\alpha_{P3,k} + F_{12,k}\alpha_{Q3,k} \\ F_{21,k}\alpha_{P3,k} + F_{22,k}\alpha_{Q3,k} \\ F_{11,k}\alpha_{P4,k} + F_{12,k}\alpha_{Q4,k} \\ F_{21,k}\alpha_{P4,k} + F_{22,k}\alpha_{Q4,k} \end{bmatrix}. \tag{18}$$

Here, the subscript "k" denotes the k^{th} converter, and $k < n$. For the last two rows of the matrix, the coefficients are as

$$\begin{bmatrix} A_{2n-1,2n-1} \\ A_{2n-1,2n} \\ A_{2n,2n-1} \\ A_{2n,2n} \end{bmatrix} = \begin{bmatrix} G_{LPF,total}(s)\left[2V_{total}\cos\theta_f - V_g\cos(\theta_{total}+\theta_f)\right]/|Z_f| \\ G_{LPF,total}(s)E_{total}V_g\sin(\theta_{total}+\theta_f)/|Z_f| + s/k_{D,p} \\ G_{LPF,total}(s)\left[2E_{total}\sin\theta_f - V_g\sin(\theta_{total}+\theta_f)\right]/|Z_f| + 1/k_{D,q} \\ -G_{LPF,total}(s)E_{total}V_g\cos(\theta_{total}+\theta_f)/|Z_f| \end{bmatrix}. \tag{19}$$

Based on (17)−(19), the root loci of the islanded 3-cell series PVBH system are shown in Figs. 6−8 with the parameters shown in Table II, unless otherwise noted. The root locus results are provided for three cases:

Case 1: Fig. 6 shows the performance of the system when the control parameters for PV converters vary. As shown in Fig. 6(a), the system has 13 poles, with λ_1 and λ_2, λ_3 and λ_4, λ_5 and λ_6, λ_7 and λ_8, λ_9 and λ_{10}, and λ_{11} and λ_{12} being conjugate pole pairs. All poles are in the left half plane, indicating that the system is stable. When $k_{p,p}$ and $k_{p,q}$ for all PV converters change from 0.06 to 0.3, only λ_9, λ_{10} and λ_{13} are fixed while other nine poles are moving. Since λ_7–λ_{13} are far from the imaginary axis compared with λ_1–λ_6, they have negligible impact on the dynamics. Thus, only the behaviors of dominant poles (λ_1–λ_6) are studied in the following.

The zoomed-in plots of Fig. 6(a) are shown in Fig. 6(b), where the loci of λ_1–λ_6 are demonstrated. With the increase of $k_{p,p}$ and $k_{p,q}$, λ_1 and λ_2 move towards the imaginary axis, leading to a smaller stability margin. On the other hand, the increase of $k_{p,p}$ and $k_{p,q}$ will drive λ_3–λ_6 away from the imaginary axis, while the damping ratio also increases.

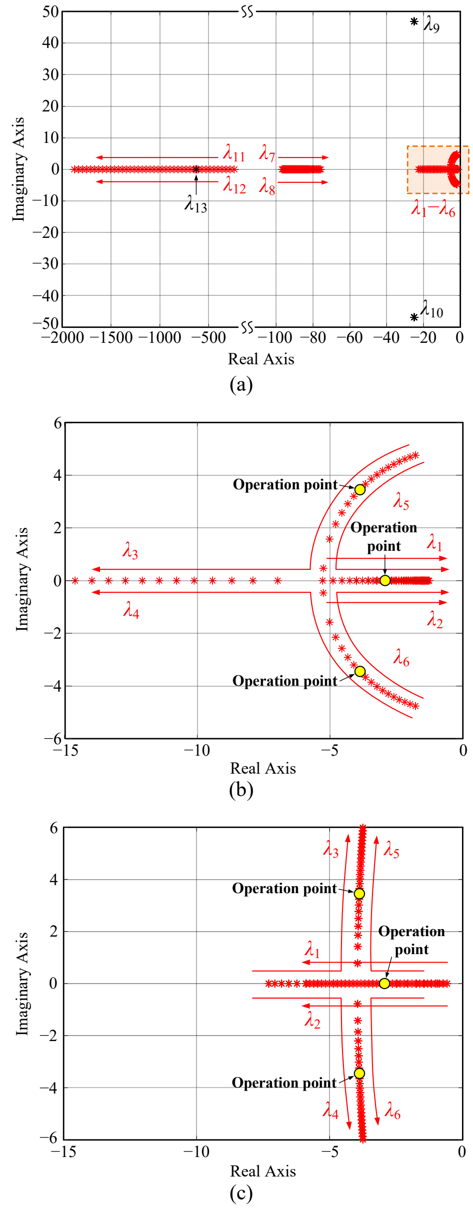

Fig. 6. Root loci diagrams for the islanded system when the control parameters of PV converters vary: (a) $k_{p,p}$ and $k_{p,q}$ for all PV converters change from 0.06 to 0.3, (b) zoomed-in plot of Fig. 6(a), and (c) zoomed-in diagram when $k_{i,p}$ and $k_{i,q}$ for all PV converters change from 0.08 to 0.8.

However, when further increasing $k_{p,p}$ and $k_{p,q}$, λ_5 and λ_6 will be closer to the imaginary axis, leading to a reduced stability margin. On the contrary, the increases of the integral gains have opposite effect on the root loci of λ_1–λ_6, as shown in Fig. 6(c). The increase of $k_{i,p}$ and $k_{i,q}$ will push λ_1 and λ_2 away from the imaginary axis, while making λ_3–λ_6 less dampened. Thus, to meet the requirements of both the stability margin and damping performance, the proportional and integral coefficients of the power loops for PV converters are selected as shown in Table II, and the operating points under the selected parameters are also highlighted in Figs. 6(b) and (c).

Case 2: To assess the stability performance when the control parameters of the battery converter vary, root loci

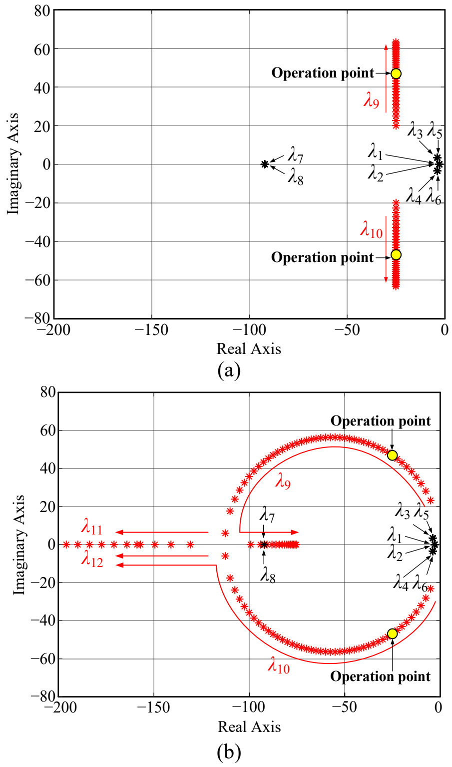

Fig. 7. Root loci diagrams for the islanded system when the control parameters of the battery converter vary: (a) $k_{D,p}$ changes from $2.28\cdot10^{-5}$ rad/(W·s) to $1.03\cdot10^{-4}$ rad/(W·s), and (b) $\omega_{cut,total}$ changes from 10 rad/s to 300 rad/s.

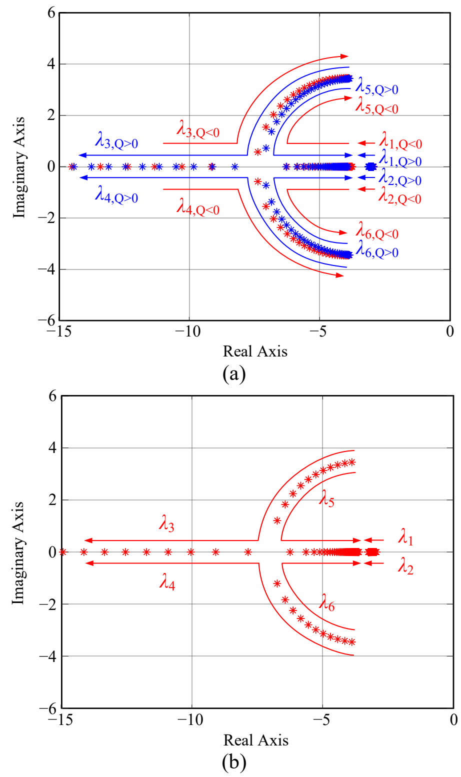

Fig. 8. Root loci diagrams for the islanded system when steady states varies: (a) V_{total} changes from 296 V to 326 V, and (b) θ_{total} changes from 0.02 rad to 0.12 rad.

when $k_{D,p}$ and $\omega_{cut,total}$ are changed are shown in Figs. 7(a) and (b), respectively. It can be seen from Fig. 7(a) that the variation of $k_{D,p}$ only affects the locations of λ_9 and λ_{10}. With the increase of $k_{D,p}$, λ_9 and λ_{10} will become less dampened. On the other hand, when $\omega_{cut,total}$ is small, λ_9 and λ_{10} are very close to the imaginary axis, indicating that the droop control will have a more significant influence on the system performance, since λ_9 and λ_{10} will become dominant. With the increase of $\omega_{cut,total}$, λ_9 and λ_{10} will move away from the imaginary axis, while their damping ratios firstly increase and then decrease. When further increasing $\omega_{cut,total}$, λ_{10} will move far away from the imaginary axis, while λ_9 will move in the opposite direction. Overall, the increase of $\omega_{cut,total}$ will lead to better stability performance.

It can be observed from Fig. 7 that λ_1–λ_6 are still the dominant poles when $k_{D,p}$ and $\omega_{cut,total}$ change. This indicates that the control parameters of the battery converter have less impact on the dynamic power sharing performance. The power sharing control between the series converters and the power control of the entire system are well decoupled. Moreover, although the variation of $\omega_{cut,total}$ will also affect the locations of λ_{11} and λ_{12}, their impact is relatively minor since they are far from the imaginary axis. In addition, the variation of $k_{D,q}$ has no effect on the root loci. Therefore, to meet the requirements of both stability and dynamics, $k_{D,p}$ and $\omega_{cut,total}$ are selected as $6.28\cdot10^{-5}$ rad/(W·s) and 50 rad/s, respectively. It should be mentioned that the selection of $k_{D,p}$ is also dependent on the requirements of the islanded grid. When designing $k_{D,p}$, it is recommended to select an appropriate value considering these requirements, and then evaluate the stability performance. The corresponding operation points are also highlighted on the root loci plots in Fig. 7.

Case 3: It can be deduced from (19) that the steady-state conditions will also affect the locations of the closed-loop poles. Thus, to evaluate the stability performance of the system under different steady states, Fig. 8 demonstrates the root loci when V_{total} and θ_{total} change. As shown in Fig. 8, λ_1–λ_6 are all located on the left half plane, meaning that the system is stable under different steady states. When V_{total} increases from 296 V to 311 V, λ_5 and λ_6 firstly move away from the imaginary axis, and then go back towards the imaginary axis with increased damping ratios, as shown in the root loci with the "Q<0" subscript in Fig. 8(a). Meanwhile, λ_5 and λ_6 keep moving towards the imaginary axis with increased damping ratios. The root loci is similar with that when θ_{total} changes from 0.02 rad to 0.12 rad, as shown in Fig. 8(b). When V_{total} further increases from 311 V to 326 V, as shown in the root loci with the "Q>0" subscript in Fig. 8(a), it almost coincides with the root loci when V_{total} increases from 296 V to 311 V, except that λ_3–λ_6 are moving in the opposite direction, compared to the former root loci in Fig. 8(a). On the other hand, the locations of λ_1 and λ_2 are hardly affected by the variations of V_{total} and θ_{total}. From the above analysis, it is clear that although the system is stable, the dynamic performance varies under different steady-state conditions. Therefore, when designing the control parameters for the individual power loops, it is essential to evaluate the stability of the system under different steady-state conditions.

From the above discussion, it can be concluded that with the properly selected control parameters, the system can be operated with satisfactory stability and dynamic performance. Moreover, it should be mentioned that all poles are fixed under different values of E_k and θ_k. Therefore, the stability performance of the system is irrelevant with the steady-state operating points of individual PV converters.

IV. Over Modulation Issues

For the series system, the main causes of the over-modulation for both the PV converters and the battery converter are explained as follows:

1) Over-modulation of PV converters: The over-modulation of PV converters is usually induced by the reduction of the line current. The detailed analysis has been discussed in [21] and [24]. Due to the MPPT control, when the line current reduces, the output voltage of the PV converter will become higher in amplitude to maintain operating at the maximum power point (MPP), and this may lead to over-modulation of PV converters.

2) Over-modulation of the battery converter: The over-modulation of the battery converter will appear when the battery converter is contributing more power than PV converters. When the battery converter is providing more active power, it generally means that the PV power is not sufficient. In this case, the over-current protection should always be triggered to protect the series system from overloading. Although heavy load active power is beyond consideration, over-modulation may also appear. As shown in Fig. 9, if the reactive power of the series system is large while the active power is relatively small, since the PV cells are operating in the MPPT mode, almost no reactive power will be contributed by the PV converters according to (7)−(9). In this case, the battery cell should not only absorb the surplus active power from PV cells, but also independently provide all the reactive power. Therefore, the battery converter will be at the risk of being over-modulated.

To address the over-modulation issues, two AOM loops are respectively developed for PV converters and the battery converter, as shown in Fig. 10. The basic idea of the AOM loops is to partially discard PV power by moving the operating points of PV units from their MPPs to the higher voltage region. This effort has three benefits:

1) Magnitudes of the modulation indices for PV converters will be reduced due to the lower PV power.
2) The available DC voltages will become higher for PV converters, making the series system generate a higher AC voltage [21].
3) With the reduction of the PV power, PV converters will contribute more reactive power according to (7)−(9), and the voltage amplitude of the battery converter can thus be reduced. If the battery is operating in the charging mode, the reduction of PV power will also reduce the charging power of the battery converter, and thereby reducing the amplitude of the modulation index for the battery converter.

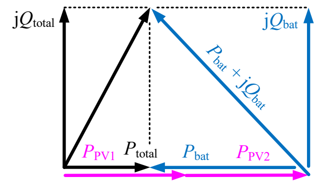

Fig. 9. Phasor diagram of the system under the over-modulation due to a low PF.

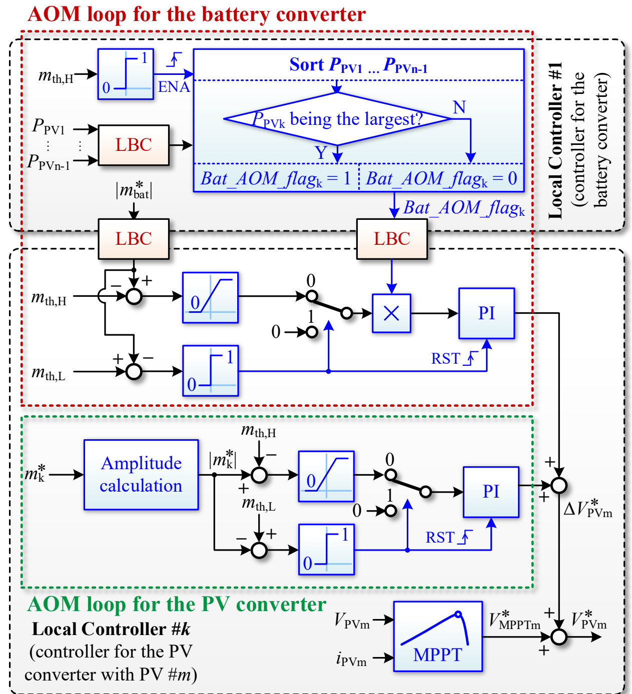

Fig. 10. Two anti-over-modulation loops, where $V^*_{\mathrm{MPPT},m}$ is the voltage reference generated by the MPPT controller of PV #*m*, and $\Delta V^*_{\mathrm{PV}m}$ is the sum of the outputs of the two AOM loops, which are implemented in the PV converter #*m*.

Based on the above, the first AOM loop is designed to address the over-modulation issues of the PV converters. As shown in Fig. 10, if $|m^*_k|$ (the amplitude of the modulation index for the k^{th} PV converter) is higher than a threshold $m_{th,H}$, a voltage increment will be added on the PV voltage reference that is calculated by a PI controller. When $|m^*_k|$ reduces, e.g., lower than a threshold $m_{th,L}$ ($m_{th,L} < m_{th,H}$), the PV converter is regarded free from the over-modulation risk. Subsequently, the PI regulator will be reset, and the PV converter starts to operate in the MPPT mode.

The AOM loop for the battery converter is implemented similarly. As shown in Fig. 10, if $|m^*_{bat}|$ (the amplitude of the modulation index for the battery converter) is higher than $m_{th,H}$, while the power of the k^{th} PV is the highest among all PV converters, an increment from a PI regulator is added on the voltage reference of the k^{th} PV. In this AOM loop, only the PV with the highest power will be selected to discard part of its power. When $|m^*_{bat}|$ is lower than $m_{th,L}$, the PI regulator will be reset, meaning that the battery converter is free from the over-modulation risk.

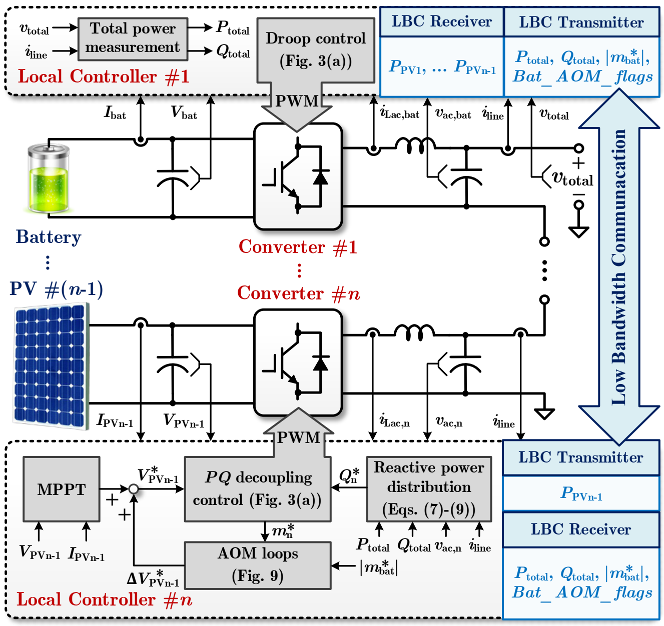

Fig. 11. Overall diagram of the proposed distributed control, where I_{bat} and $I_{PV,n-1}$ refer to the DC current of the battery and PV # (n-1), respectively, and $i_{Lac,bat}$ and $i_{Lac,n}$ are the currents on the AC filter inductors of the battery converter and the n^{th} converter, respectively.

Notably, the two AOM loops are all implemented in each PV converter, as shown in Fig. 10, while the battery converter is responsible for collecting the PV power data of all PV converters, and determining whether the AOM loop of the battery converter is activated for certain PV converters. Due to the introduction of the two AOM loops, more variables should be transmitted by the LBC, which are $|m^*_{bat}|$, PV power information (P_{PV1}, … P_{PVn-1}), and the enabling flags of the AOM loop for the battery converter, as shown in Fig. 10. Nevertheless, as the AOM loops and the transmitted variables have very slow dynamics, the LBC system will still be sufficient. In addition, all the enabling flags of the AOM loop for the battery converter, denoted as Bat_AOM_flag$_k$ (the subscript "k" indicates that this flag is assigned to the k^{th} converter), can be combined as one variable to further reduce the communication burden. Therefore, the AOM loops have a negligible impact on the communication burden of the series system. Overall, the diagram of the proposed distributed control is shown in Fig. 11, which demonstrates the locations of all the aforementioned and all necessary communicating variables.

V. EXPERIMENTAL RESULTS

To validate the effectiveness of the proposed control, experiments have been performed on a down-scaled 3-cell series PVBH system, as shown in Fig. 12, which is assembled with three Infineon FS50R12KT4_B15 IGBT modules. One Keysight E4360A PV simulator was used to provide the power supply for two PV converters, and one Delta Elektronika SM330 DC power supply paralleling with a resistor bank is adopted to mimic the battery. Three TMS320F28335 digital signal processors were employed as individual controllers, which are interlinked with the RS-485 serial communication. The experimental parameters are the same with Table II, except that the nominal peak AC voltage is reduced to 64 V due to the limited output voltage of the PV simulator. Additional parameters of the experiments are listed in Table III, where the control parameters of the AOM loops are also included.

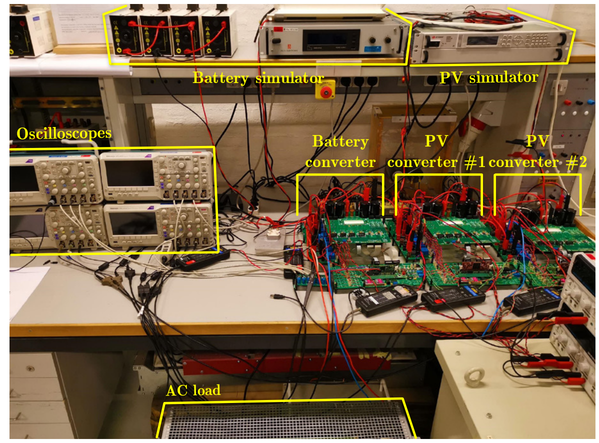

Fig. 12. Prototype of the down-scaled series PVBH system.

TABLE III
PARAMETERS OF THE EXPERIMENTS.

Circuit parameters	Value
PV rated power	260 W
Output LC filter of one cell	1.8 mH / 30 μF
DC link capacitor	2000 μF
Amplitude of the nominal grid voltage $V_{g,nom}$	90 V
Nominal voltage of the battery	48 V
Control parameters	**Value**
Switching frequency	5 kHz
Controller sampling frequency	10 kHz
MPPT sampling-rate	5 Hz
MPPT step-size	2.5 V
Reactive power distribution coefficient h	2.8
Proportional gain of the AOM loop for PV converters	$k_{p,AOM,PV}$ = 50
Integral gain of the AOM loop for PV converters	$k_{q,AOM,PV}$ = 500
Proportional gain of the AOM loop for PV converters	$k_{p,AOM,bat}$ = 30
Integral gain of the AOM loop for PV converters	$k_{q,AOM,bat}$ = 100
Upper threshold	$m_{th,H}$ = 0.9
Lower threshold	$m_{th,L}$ = 0.8
Communication baud rate	9600 bps

Test 1: The performance of the islanded system during load active power step change is demonstrated in Figs. 13 and 14, where the load active power jumps from 625 W to 165 W, while the reactive power remains at 0. As shown in Fig. 13, before the load change, the active power of each PV converter is approximately 225 W, and the remaining 175-W active power is supported by the battery converter. The PV converters are operating at their MPPs, which can be confirmed by Fig. 14(a), where the PV voltages oscillate around 55 V. The 35-W power loss is due to the converter losses. After the load change, the power of the two PV

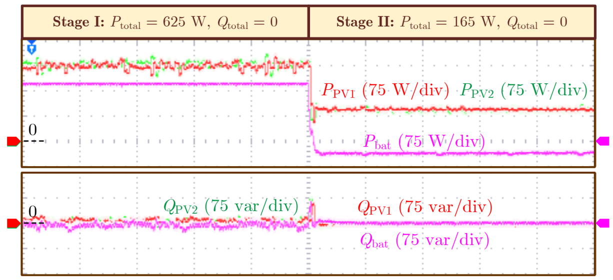

Fig. 13. Power control performance of the series PVBH system during load active power step change.

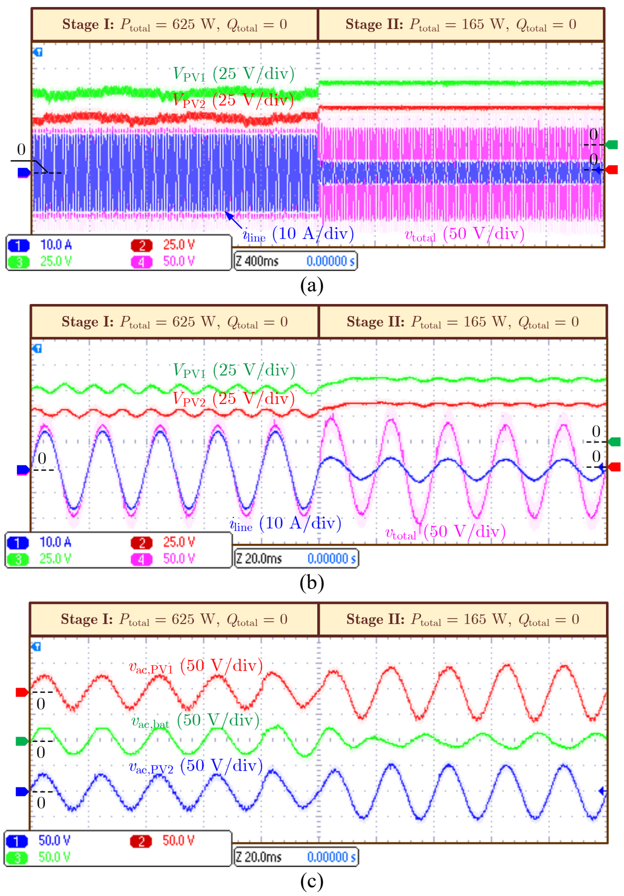

Fig. 14. Voltage and current response of the series PVBH system during load active power step change: (a) PV voltages, grid voltage and current, (b) zoomed-in plot of Fig. 14(a), and (c) output voltages of the three converters.

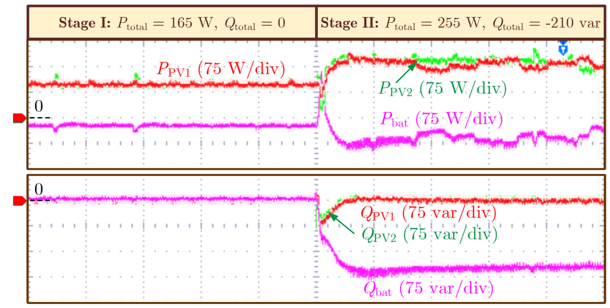

Fig. 15. Power control performance of the series PVBH system during load active and reactive power step change.

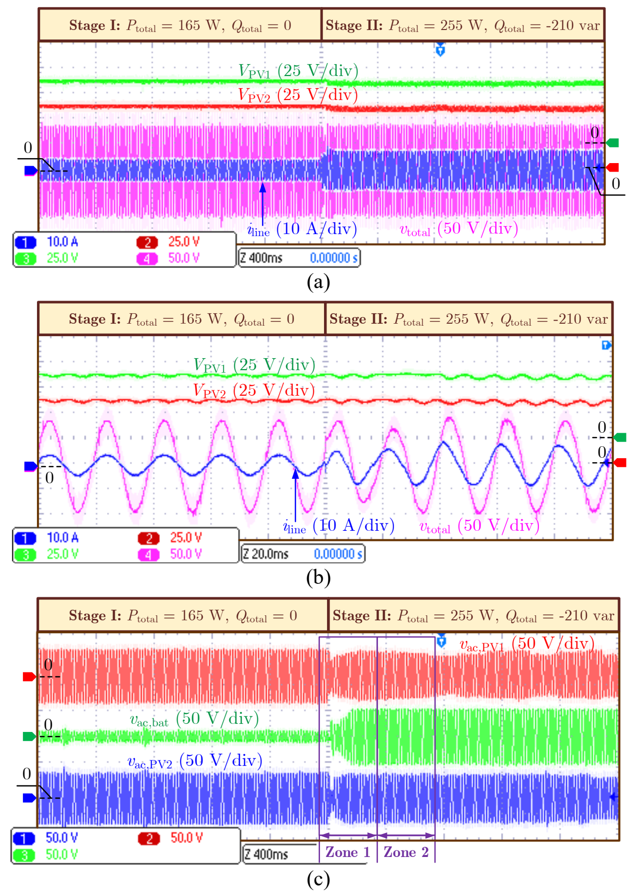

Fig. 16. Voltage and current response of the series PVBH system during load active and reactive power change: (a) PV voltages, grid voltage and current, (b) zoomed-in plot of Fig. 16(a), and (c) output voltages of the three converters.

converters is reduced to 95 W, while the surplus 35-W active power is absorbed by the battery. Due to the reduction of the line current, the PV voltages are raised to 62 V to avoid over-modulation of PV converters, as shown in Figs. 14(a) and (b), and the output voltage of the battery converter has a reversed polarity, as shown in Fig. 14(c), indicating that the battery is operating in the charging mode. During the entire process, the reactive power of each converter is kept approximately at zero. Despite the slight overshooting at the beginning of the load change, the total AC voltage of the islanded system is stable and of high quality, as seen in Fig. 14(b).

Test 2: The reactive power control performance of the series PVBH system is shown in Figs. 15−17, where the load power changes from 165 W and 0 var to 255 W and −210 var. As shown in Fig. 15, after the load change, the power of PV converters is increased to approximately 160 W, and the battery is charged at around 65 W. Most load reactive power is supported by the battery, being around −190 var in steady state, while each PV converter only has −10 var reactive power. The apparent power can be calculated from the experimental results, being about 200 VA for the battery converter, and 160 VA for PV converters. Since more reactive power is provided by the battery converter, over-modulation appears after the load change, as shown in Fig. 16(c) and Fig. 17. However, due to the implementation of the AOM loop for the battery converter, the over-modulation is then

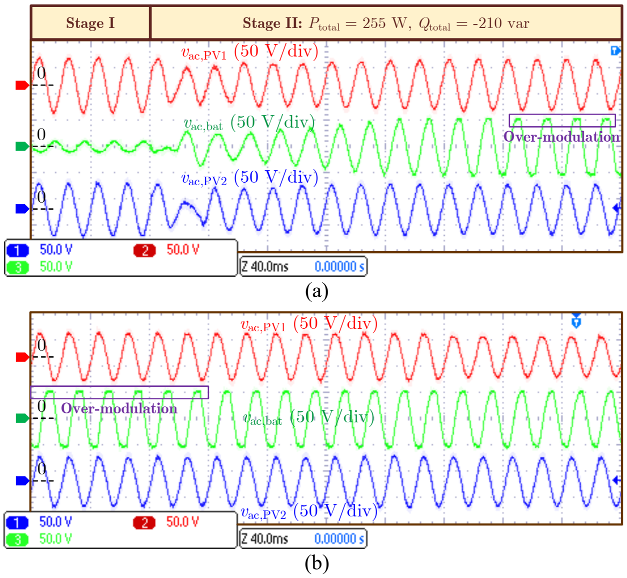

Fig. 17. Output voltages of the three converters: (a) zoomed-in plot of Zone 1 and (b) zoomed-in plot of Zone 2 in Fig. 16(c).

alleviated after several cycles, as shown in Fig. 17(b). The grid voltage is kept stable, except for the first two cycles after the load change, where an approximately 20% grid voltage drop occurs, as shown in Figs. 16(a) and (b).

Test 3: To better demonstrate the performance of the reactive power distribution scheme, experimental results are provided in Figs. 18 and 19, where the load conditions are the same with Test 2, while the maximum PV power is reduced by a half. As it can be observed from Fig. 18, before the load change, the active power of each PV converter is around 90 W, while the battery is charged at about 15 W. After the load change, the active power from each PV converter increases to around 120 W, and the remaining 15-W active power is provided by the battery. Due to the increase of the line current, the operating points of the two PV converters move back to their MPPs, as shown in Fig. 19(a), where the PV voltages are oscillating around 55 V. Reactive power is distributed according to the active power contribution of each converter, as shown in Fig. 18, where most reactive power is supported by the battery converter, being around −150 var in steady state, while the reactive power for each PV converter is around −30 var. The apparent power of each converter can accordingly be calculated, being 150.7 VA and 123.7 VA for the battery converter and each PV converter, respectively. The distribution of the apparent power can be confirmed by the output voltages of the three converters, as shown in Fig. 19(c), where the output voltages of all three converters are roughly equal, while the output voltage of the battery converter has a larger amplitude. During the entire process, the islanding AC voltage is stable and of high quality, despite the voltage dip and overshooting appearing in the first two cycles after the load change, as shown in Figs. 19(a) and (b).

Overall, the effectiveness of the proposed *PQ* decoupling control, reactive power distribution scheme, and the two AOM loops have been validated by the experimental results. The distributed control of the series PVBH system can be achieved

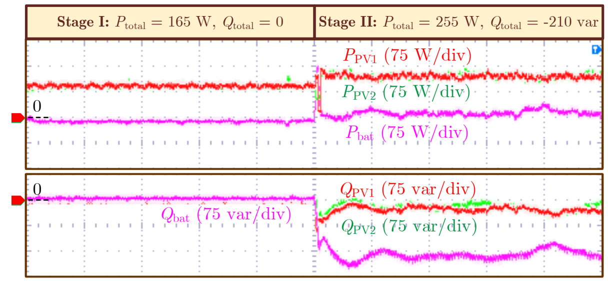

Fig. 18. Power control performance of the series PVBH system during load active and reactive power change when PV power is halved.

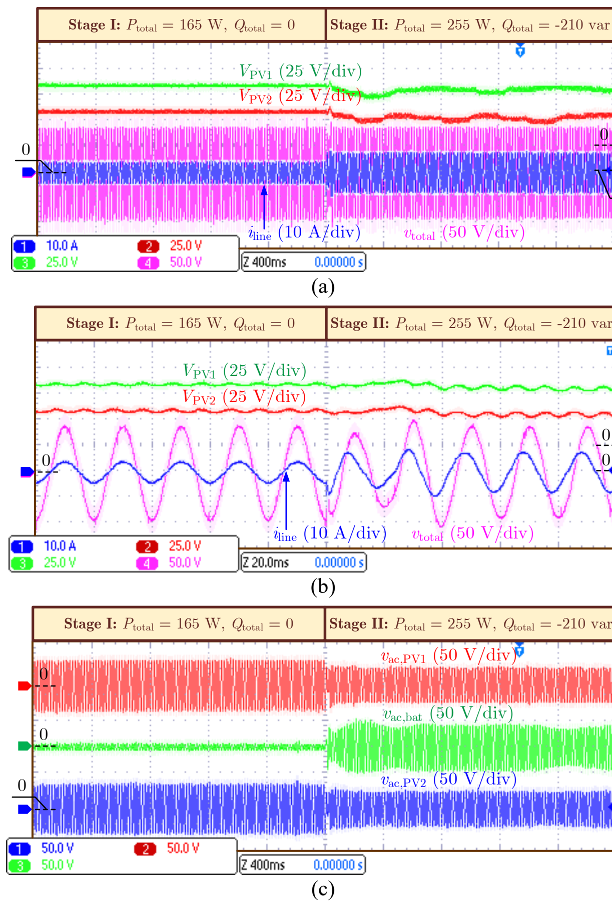

Fig. 19. Voltage and current response of the series PVBH system during load active and reactive power change when PV power is halved: (a) PV voltages, grid voltage and current, (b) zoomed-in plot of Fig. 19(a), and (c) output voltages of the three converters.

with very low communication burden. However, according to the experimental results in Tests 2 and 3, it is obvious that the reactive power distribution performance is not optimized. The battery contributes more reactive power, as discussed in Section II. In order to obtain better reactive power distribution performance, the reactive power reference of each converter can be calculated with the implementation of certain optimization algorithms, which will inevitably increase the computation cost. Nevertheless, the proposed reactive power distribution scheme remains a cost-effective solution to balancing the loading of all converters.

Finally, to demonstrate the performance of the proposed method in terms of communication burden reduction, the

TABLE IV
COMPARISONS OF THE LBC PARAMETERS BETWEEN THE CONVENTIONAL AND PROPOSED CONTROL METHODS.

Parameters / Methods	Necessary communication variables		Communication protocol	Baud-rate in experiments
	Real-time transmission not required	Real-time transmission required		
Conventional methods based on the hierarchical control [20], [21]	P_{PV1}, … P_{PVn-1}, P_{bat}, Q_1^* … Q_{n-1}^*, V_{PV1}, … V_{PVn-1}, V_{bat}, $\lvert m_{bat}^* \rvert$ (3n variables in total)	$\lvert m_{total}^* \rvert$[a], $\Delta\theta_{mtotal}$[b], $\Delta M_{p,1}$, … $\Delta M_{p,n-1}$[c], $\Delta M_{q,1}$, … $\Delta M_{q,n-1}$[d] (2n variables in total)	CAN	1M bps
Proposed control	P_{total}, Q_{total}, $\lvert m_{bat}^* \rvert$, P_{PV1}, … P_{PVn-1}, *Bat_AOM_Flags*[e] (n + 3 variables in total)	null	RS-485	9600 bps

[a] $\lvert m_{total}^* \rvert$ is the amplitude of m_{total}^*, which is the total modulation index (calculated by the PQ control in the central controller) [21].
[b] $\Delta\theta_{mtotal} = \theta_{mtotal} - \theta_L$, where θ_{mtotal} is the phase angle of m_{total}^*, and θ_L is the phase-angle of the line current [21].
[c,d] $\Delta M_{p,k}$ and $\Delta M_{q,k}$ are the adjustments on the modulation index of the k^{th} converter, which are calculated by local active power and reactive power controllers, respectively [21].
[e] All *Bat_AOM_Flag*s can be considered as one communication variable, as explained in Section IV.

communication parameters between the conventional hierarchical control and the proposed approach are compared in Table IV. As shown in Table IV, when using the conventional methods to accomplish the same function with the proposed control, a total number of 5n variables should be transmitted for an n-cell series PVBH system, among which 2n variables should be real-time transmitted. On the other hand, the total number of transmitted variables is reduced to (n + 3), and none of them should be real-time transmitted. Although different communication protocols have been employed in the experiments, being the controller area network (CAN) and RS-485 for the conventional and the proposed control, respectively, the baud-rate of the proposed method (9600 bps) is much lower than the conventional solutions (1 Mbps). Therefore, from the above discussion, it can be concluded that the communication burden can be significantly reduced compared with the conventional hierarchical control.

VI. CONCLUSIONS

A novel distributed control for series PVBH systems in islanded operation was proposed in this paper. Firstly, a *PQ* decoupling control was introduced, enabling the individual *PQ* control of each converter with only local measurements. Then, a droop controller was implemented in the local controller of the battery converter, making the series system able to participate in voltage and frequency regulation of the islanded grid. A reactive power distribution scheme was proposed to balance the loading of all converters. To prevent the over-modulation, two AOM loops were developed. The proposed control can be realized with very low communication burden, where only several variables with slow dynamics should be transmitted by the LBC. Compared with conventional approaches, the proposed control can cope with more complicated operation conditions with stronger communication fault tolerance. Experimental results have validated the effectiveness of the proposed method.

REFERENCES

[1] Y. Yang, K. A. Kim, F. Blaabjerg, and A. Sangwongwanich, *Advances in Grid-Connected Photovoltaic Power Conversion Systems*, Publisher: Woodhead Publishing, 2018.

[2] J. He, Y. Li, C. Wang, Y. Pan, C. Zhang, and X. Xing, "Hybrid microgrid with parallel- and series-connected microconverters," *IEEE Trans. Power Electron*., vol. 33, no. 6, pp. 4817-4831, June 2018.

[3] L. Liu, H. Li, Z. Wu, and Y. Zhou, "A cascaded photovoltaic system integrating segmented energy storages with self-regulating power allocation control and wide range reactive power compensation," *IEEE Trans. Power Electron*., vol. 26, no. 12, pp. 3545-3559, Dec. 2011.

[4] W. Jiang, S Xue, L. Zhang, W. Xu, K. Yu, W. Chen, and L. Zhang, "Flexible power distribution control in an asymmetrical-cascaded-multilevel-converter-based hybrid energy storage system," *IEEE Trans. Ind. Electron.*, vol. 65, no. 8, pp. 6150-6159, Aug. 2018.

[5] B. Xiao, L. Hang, J. Mei, C. Riley, L. M. Tolbert, and B. Ozpineci, "Modular cascaded H-bridge multilevel PV inverter with distributed MPPT for grid-connected applications," *IEEE Trans. Ind. Appl*., vol. 51, no. 2, pp. 1722-1731, Mar./Apr. 2015.

[6] A. Marquez, J. I. Leon, S. Vazquez, L. G. Franquelo, and S. Kouro, "Operation of an hybrid PV-battery system with improved harmonic performance," in *Proc. 43rd Annu. Conf. IEEE Ind. Electron. Soc*., 2017, pp. 4272–4277.

[7] Y. Pan, A. Sangwongwanich, Y. Yang, and F. Blaabjerg, "A phase-shifting MPPT to mitigate interharmonics from cascaded H-bridge PV inverters," *IEEE Trans. Ind. Appl*., DOI: 10.1109/TIA.2020.3000969.

[8] L. Zhang, K. Sun, Y. W. Li, X. Lu, and J. Zhao, "A distributed power control of series-connected module-integrated inverters for PV grid-tied applications," *IEEE Trans. Power Electron*., vol. 33, no. 9, pp. 7698-7707, Sept. 2018.

[9] H. Jafarian, S. Bhowmik, and B. Parkhideh, "Hybrid current-/voltage-mode control scheme for distributed AC-stacked PV inverter with low-bandwidth communication requirements," *IEEE Trans. Ind. Electron.*, vol. 65, no. 1, pp. 321-330, Jan. 2018.

[10] H. Jafarian, R. Cox, J. H. Enslin, S. Bhowmik, and B. Parkhideh, "Decentralized active and reactive power control for an AC-stacked PV inverter with single member phase compensation," *IEEE Trans. Ind. Appl*., vol. 54, no. 1, pp. 345-355, Jan.-Feb. 2018.

[11] N. Kim and B. Parkhideh, "Control and operating range analysis of an AC-stacked PV inverter architecture integrated with a battery," *IEEE Trans. Power Electron*., vol. 33, no. 12, pp. 10032-10037, Dec. 2018.

[12] P.-H. Wu, Y.-C. Su, J.-L. Shie, and P.-T. Cheng, "A distributed control technique for the multilevel cascaded converter," *IEEE Trans. Ind. Appl*., vol. 55, no. 2, pp. 1649-1657, Mar.-Apr. 2019.

[13] J. He, Y. Li, B. Liang, and C. Wang, "Inverse power factor droop control for decentralized power sharing in series-connected-microconverters-based islanding microgrids," *IEEE Trans. Ind. Electron*., vol. 64, no. 9, pp. 7444-7454, Sept. 2017.

[14] Y. Sun, G. Shi, X. Li, W. Yuan, M. Su, H. Han, and X. Hou, "An f-P/Q droop control in cascaded-type microgrid," *IEEE Trans. Power Syst*., vol. 33, no. 1, pp. 1136-1138, Jan. 2018.

[15] X. Hou, Y. Sun, H. Han, Z. Liu, W. Yuan, and M. Su, "A fully decentralized control of grid-connected cascaded inverters," *IEEE Trans. Sustain. Energy*, vol. 10, no. 1, pp. 315-317, Jan. 2019.

[16] Y. Sun, L. Li, G. Shi, X. Hou, and M. Su, "Power factor angle droop control−a general decentralized control of cascaded inverters," *IEEE Trans. Power Del*., vol. 36, no. 1, pp. 465-468, Feb. 2021.

[17] X. Hou, Y. Sun, H. Han, Z. Liu, M. Su, B. Wang, and X. Zhang, "A general decentralized control scheme for medium-/high-voltage

cascaded STATCOM," *IEEE Trans. Power Syst.*, vol. 33, no. 6, pp. 7296-7300, Nov. 2018.

[18] J. He, Y. Liu, and Y. Wang, "Cascaded droop and inverse droop regulation for two-layer coordinated power flow control in series-connected power cells," *IEEE Trans. Ind. Electron.*, DOI: 10.1109/TIE.2020.3005099.

[19] *IEEE Standard for Interconnection and Interoperability of Distributed Energy Resources with Associated Electric Power Systems Interfaces*, IEEE Standard 1547-2018, Apr. 2018.

[20] Y. Pan, C. Zhang, S. Yuan, A. Chen, and J. He, "A decentralized control method for series connected PV battery hybrid microgrid," in *Proc. IEEE Transp. Electrific. Conf. Expo, Asia-Pacific (ITEC Asia-Pacific)*, Aug. 2017, pp. 1–6.

[21] Q. Zhang and K. Sun, "A flexible power control for PV-battery hybrid system using cascaded H-bridge converters," *IEEE J. Emerg. Sel. Topics Power Electron*., vol. 7, no. 4, pp. 2184-2195, Dec. 2019.

[22] H. Liao, X. Zhang, and X. Hou, "A decentralized control of series-connected PV-ES inverters with MPPT and virtual inertia functionality," in *Proc. IEEE APEC Expo*., Mar. 2020, pp. 3221-3224.

[23] S. Das, I. U. Nutkani, and C. Teixeira, "Autonomous power management of series-parallel hybrid microgrid," in *Proc. IEEE ICPES*, 2019, pp. 1-6.

[24] T. Zhao, X. Zhang, W. Mao, F. Wang, J. Xu, Y. Gu, and X. Wang, "An optimized third harmonic compensation strategy for single-phase cascaded H-bridge photovoltaic inverter," *IEEE Trans. Ind. Electron.*, vol. 65, no. 11, pp. 8635-8645, Nov. 2018.

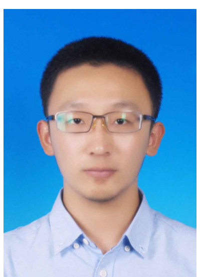

Yiwei Pan (S'19) received the B.S. degree in automation and M.S. degree in power electronics from Shandong University, Ji'nan, China, in 2015 and 2018, respectively. He is currently working toward the Ph.D. degree at Aalborg University, Aalborg, Denmark. From July 2016 to May 2018, he was an exchange student with Tianjin University, China.

His current research interests include multilevel converters and distributed power generation. He was the recipient of the Best Paper Award at IPEMC-ECCE Asia 2020.

Ariya Sangwongwanich (S'15−M'19) received the M.Sc. and Ph.D. degree in energy engineering from Aalborg University, Denmark, in 2015 and 2018, respectively. Currently, he is working as a Postdoc Fellow at the Department of Energy Technology, Aalborg University.

He was a Visiting Researcher with RWTH Aachen, Aachen, Germany from September to December 2017. His research interests include control of grid-connected power converters, photovoltaic systems, reliability in power electronics and multilevel converters. In 2019, he received the Danish Academy of Natural Sciences' Ph.D. prize and the Spar Nord Foundation Research Award for his Ph.D. thesis.

Yongheng Yang (SM'17) received the B.Eng. degree in Electrical Engineering and Automation from Northwestern Polytechnical University, China, in 2009 and the Ph.D. degree in Energy Technology from Aalborg University, Denmark, in 2014. He was a postgraduate student with Southeast University, China, from 2009 to 2011. In 2013, he spent three months as a Visiting Scholar at Texas A&M University, USA. Since 2014, he has been with the Department of Energy Technology, Aalborg University, where he became a tenured Associate Professor in 2018. In January 2021, he joined Zhejiang University, China, where he is now a ZJU100 Young Professor at the Department of Electrical Engineering.

Dr. Yang was the Chair of the IEEE Denmark Section (2019-2020). He is the secretary for the Technical Committee of Sustainable Energy Systems (TC5) of the IEEE PELS. He is an Associate Editor for several IEEE Transactions/Journals and a Deputy Editor of the *IET Renewable Power Generation* for Solar Photovoltaic Systems. He received the 2018 *IET Renewable Power Generation* Premium Award and was an Outstanding Reviewer for the IEEE TRANSACTIONS ON POWER ELECTRONICS in 2018. In addition, he has received two IEEE Best Paper Awards. His current research is to tackle the issues brought by the integration of photovoltaic systems and multi-energy vectors through developing reliable and efficient power converters with advanced control.

Frede Blaabjerg (S'86–M'88–SM'97–F'03) was with ABB-Scandia, Randers, Denmark, from 1987 to 1988. From 1988 to 1992, he got the PhD degree in Electrical Engineering at Aalborg University in 1995. He became an Assistant Professor in 1992, an Associate Professor in 1996, and a Full Professor of power electronics and drives in 1998. From 2017 he became a Villum Investigator. He is honoris causa at University Politehnica Timisoara (UPT), Romania and Tallinn Technical University (TTU) in Estonia.

His current research interests include power electronics and its applications such as in wind turbines, PV systems, reliability, harmonics and adjustable speed drives. He has published more than 600 journal papers in the fields of power electronics and its applications. He is the co-author of four monographs and editor of ten books in power electronics and its applications.

He has received 32 IEEE Prize Paper Awards, the IEEE PELS Distinguished Service Award in 2009, the EPE-PEMC Council Award in 2010, the IEEE William E. Newell Power Electronics Award 2014, the Villum Kann Rasmussen Research Award 2014, the Global Energy Prize in 2019 and the 2020 IEEE Edison Medal. He was the Editor-in-Chief of the IEEE TRANSACTIONS ON POWER ELECTRONICS from 2006 to 2012. He has been Distinguished Lecturer for the IEEE Power Electronics Society from 2005 to 2007 and for the IEEE Industry Applications Society from 2010 to 2011 as well as 2017 to 2018. In 2019-2020 he serves a President of IEEE Power Electronics Society. He is Vice-President of the Danish Academy of Technical Sciences too.

He is nominated in 2014-2019 by Thomson Reuters to be between the most 250 cited researchers in Engineering in the world.